Hindawi Publishing Corporation
Shock and Vibration
Volume 2014, Article ID 397584, 18 pages
http://dx.doi.org/10.1155/2014/397584

Research Article

Design of Hybrid Dynamic Balancer and Vibration Absorber

Y. R. Wang and C. Y. Lo

Department of Aerospace Engineering, Tamkang University, Tamsui District, New Taipei City 25137, Taiwan

Correspondence should be addressed to Y. R. Wang; 090730@mail.tku.edu.tw

Received 23 February 2014; Accepted 27 June 2014; Published 17 August 2014

Academic Editor: Tony Murmu

Copyright © 2014 Y. R. Wang and C. Y. Lo. This is an open access article distributed under the Creative Commons Attribution License, which permits unrestricted use, distribution, and reproduction in any medium, provided the original work is properly cited.

This study proposed a novel hybrid dynamic balancer and vibration absorber that is cheaper than active dampers and more effective than passive dampers. The proposed damping system does not need to be altered structurally to deal with different damping targets. Rather, the proposed vibration absorber is capable of self-adjustment to the optimal damping location in order to achieve balance and, thereby, optimize damping effects. The proposed device includes a groove under the damping target with inertial mass hung from a coil spring beneath. This allows the device to bounce vertically or rotate in order to reduce vibrations in the main body. The coil spring vibration absorber can also slide along the groove in order to adjust its location continuously until the vibrations in the system are minimized and the main body is balanced. Experiments verify the efficacy of the proposed device in improving damping performance beyond what has been achieved using conventional devices. We also provide an explanation of the theoretical underpinnings of the design as well as the implications of these findings with regard to future developments.

1. Introduction

Vibration can affect the stability of a structure, and constant vibration can lead to fatigue and structural damage. Babitsky and Veprik [1] studied vibration suppression from the perspective of balance using an elastic beam with a sliding washer damping system. Their results proved that this type of self-damping system is capable of eliminating resonance and decreasing beam vibration. Another approach to maintaining balance is the ball-type automatic balancer system (ABS), comprising several balls moving along a fixed circular orbit. Under proper conditions, the balls move to specific positions of equilibrium, thereby suppressing unbalanced vibrations. The application of this approach in optical disk drives was outlined by Chao et al. [2, 3]. Lu and Hung [4] proposed the balancing of components using two or three balls. Their approach proved to be three times more effective than using a single-ball balancer system. Based on these achievements, this study sought to extend the application of free-moving components in vibrating rigid bodies for the elimination of vibration.

Vibration damping methods can roughly be divided into two types: active and passive. Generally speaking, active damping is the most effective approach to vibration damping; however, most conventional machine tools vibrate in the vertical direction, which is best dealt with using a tuned-mass damper (TMD) comprising a mass and one or more springs. The first theoretical investigation of TMD was performed by Den Hartog in 1947 [5]. Vakakis and Paipetis [6] investigated the effect of SDOF TMDs on the first mode of a MDOF primary system. Zuo and Nayfeh [7] showed that an MDOF TMD can provide higher damping in the first three flexural modes than that attained using multiple SDOF TMDs.

In general, TMDs or dynamic vibration absorbers (DVAs) are resonant devices used to damp or absorb vibration. In particular, the DVAs are undamped absorbers. Heo et al. [8] employed composite materials in vibration absorbers in the corners of an optical disk drive in order to reduce out-of-plane vibrations. Their vibration absorber comprises a steel ring and rubber bobbin, which play the roles of inertia mass and spring, respectively. Chung [9] later proposed another damping method for in-plane vibrations, involving two rubber components on the two sides of the drive. Wu et al. [10] used an active rotational pendulum vibration absorber to reduce the transverse vibration of a primary body. Varying the rotational speed of the pendulum enables

the tuning of the absorber frequency, whereupon the inertial force of the revolving mass is helpful in reducing vibration of the main body. These results have been improved upon in subsequent studies [11]. Wang and Chang [12] added a time-dependent boundary dynamic vibration absorber (TDB DVA) that was suspended at the free end of a hinged-free beam to reduce vibration and prevent internal resonance. The DVAs with various spring constants were considered and the optimal mass range for the DVA to reduce vibration in the main structure was also proposed.

Wang and Chen [13] proposed the placement of a single damper at the corner of the swash plate in a rotary wing to achieve vibration reduction by altering the location of the damper. Wang and Chang [14] investigated vibration reduction in a nonlinear support base with dual-shock-absorbers. They found that vibration reduction is more effective when the natural frequencies of the two shock absorbers are similar. This phenomenon is often observed at the endpoint of a rigid body plate when the dual-shock-absorbers are in the same position. Wang and Chang [15] proposed moving the location of the vibration absorber as a means to increase flutter speed in two-dimensional aeroelastic problems. Wang and Chen [16] studied the effects of positioning multiple dampers in a dual-plate mechanism for vibration reduction. Their experimental results demonstrated that the optimal vibration reduction effect was achieved when one of the dual TMDs was attached at a position below the point of applied force and the other one was attached at the diagonal quadrant endpoint. This combination proved to be the most effective in reducing the amplitude of vibrations of the plates. Wang and Lin [17] also proposed a set of principles for adjusting the damper location in a nonlinear two-dimensional system with 3 : 1 internal resonance. The principles are based on altering the location of the damper in order to eliminate internal resonance and flutter. These studies prove that adjusting the location of passive dampers is an effective means to reduce vibrations in the main body. Wang and Hung [18] investigated the effect of a pendulum tuned mass damper (PTMD) on the vibration of a slender two-dimensional rigid body with 1 : 2 internal resonance. They focused on the damping effect of the various parameters of the PTMD in reducing the vibration of the system. Their study indicated that without changing the main configuration, the vibration amplitudes in the main body could be greatly reduced by changing the positions and certain parameter combinations of the PTMD.

All of these studies involve one or more TMDs (or DVAs) placed at fixed locations. They present optimal damping effects under fixed external forces; however, they are not necessarily effective in dealing with external forces that change or for rotating in-plane vibrations. ABS applications provide a track to guide the movement of the damper at balancing position; however, they are unable to provide exert optimal damping effects on the vertical vibrations in general machine tools or out-of-plane vibrations. This study designed a hybrid dynamic balancer and vibration absorber (HDBVA) to reduce the vibrations in operating equipment with rigid structures. The proposed vibration absorber is simple in structure, costs less than active vibration absorbers, and need not be structurally altered to deal with variations in external forces. The vibration absorber moves along a groove when changes occur in the operating environment. The vibration absorber also balances instabilities in the main body and automatically moves to the location required for optimal damping, thereby achieving vibration reduction superior to that afforded by passive vibration absorbers. This innovation eliminates the shortcomings of existing active and passive dampers, combines the advantages of both, and elevates vibration reduction to a new level.

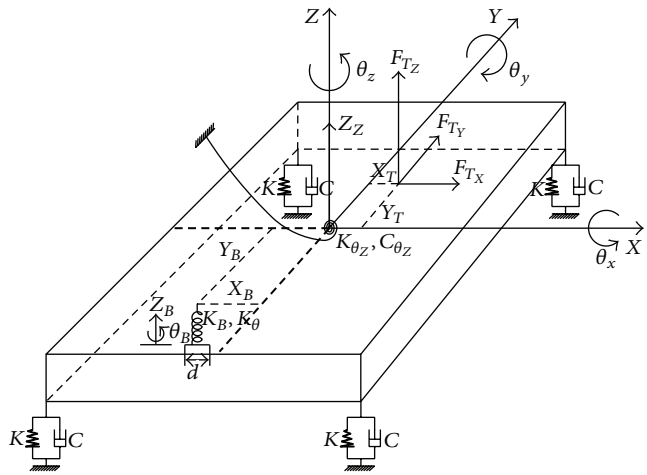

Figure 1: Theoretical model of the rigid plate with vibration absorber.

The main body in this study comprises a rigid plate, the four corners of which are fixed to an optical table using springs. Computer numerical control (CNC) was used to cut a groove on the panel to guide the movement of the vibration absorber. The application of external forces to the main body was achieved using a signal generator to send a sine wave to an actuator, which then applied the force to the rigid plate. A laser displacement gauge was used to measure vertical vibrations (z-axis) as well as the amount of rotation around the X-, Y-, and Z-axes. We also developed a theoretical model using a rigid plate as the main body, in which the four corners are supported by a combination of springs and dampers, as well as a HDBVA that can be placed at any location. Lagrange's equation was used to derive the equations of motion and obtain the amplitudes and torsion angles in each DOF. Through numerical simulation, we derived the frequency responses of each DOF and compared them with experiment results to verify the accuracy of the proposed model.

2. Structure of Theoretical Model

This section describes the development of the equations of motion using Lagrange's equation. We first defined all of the symbols and their relative positions in the system, as shown in Figure 1. M denotes the mass of the main body in the theoretical model, which is regarded as a rigid plate.

The center of the main body serves as the origin of the system. I_X and I_Y represent the mass moments of inertia in the X and Y directions. K and C are the spring constant and damping coefficient of the supports at the four corners, respectively. To simulate the in-plane degree-of-freedom of the rotational vibration around the Z-axis, we assumed that the rigid plate also has a torsional spring and damper supporting it to deal with rotation around the Z-axis, as shown in Figure 1, where K_{θ_Z} and C_{θ_Z} are the spring constant and damping coefficient of the torsional spring. X_i and Y_i ($i = 1 \sim 4$) present the distances between the origin and the four corners of the rigid plate, and X_T and Y_T signify the distance between the origin and the point of force application. Z_Z is defined as the vertical amplitude of the main body in the model, and θ_X, θ_Y, and θ_Z indicate the amount of rotation around the three axes.

As for the vibration absorber, m denotes the mass of the HDBVA mounted on the main body, and d is the radius of gyration of the HDBVA inertial mass. X_B and Y_B are the location coordinates of the HDBVA; K_B and K_θ are the extension spring constant and torsional spring constant of the HDBVA. Z_B and θ_B are the vertical amplitude and amount of rotation of the HDBVA, and δ is the coupling coefficient of the two. F_{TZ} signifies the external force, of which F_{TX} and F_{TY} represent the components of the F_{TZ} on the X- and Y-axes. The kinetic energy (T), potential energy (V), and Rayleigh dissipation function (R) of the system can be written as

$$\begin{aligned}
T &= \frac{1}{2}M\dot{Z}_Z^2 + \frac{1}{2}I_X\dot{\theta}_X^2 + \frac{1}{2}I_Y\dot{\theta}_Y^2 + \frac{1}{2}I_Z\dot{\theta}_Z^2 \\
&\quad + \frac{1}{2}I_B\dot{\theta}_B^2 + \frac{1}{2}m\dot{Z}_B^2, \\
V &= \frac{1}{2}K(Z_Z - X_1\theta_Y + Y_1\theta_X)^2 + \frac{1}{2}K(Z_Z - X_2\theta_Y + Y_2\theta_X)^2 \\
&\quad + \frac{1}{2}K(Z_Z - X_3\theta_Y + Y_3\theta_X)^2 \\
&\quad + \frac{1}{2}K(Z_Z - X_4\theta_Y + Y_4\theta_X)^2 + \frac{1}{2}K_{\theta_Z}\theta_Z^2 \\
&\quad + \frac{1}{2}K_B[Z_B - (Z_Z - X_B\theta_Y + Y_B\theta_X)]^2 \\
&\quad + \frac{1}{2}K_\theta(\theta_B - \theta_Z)^2 \\
&\quad + \frac{1}{2}\delta\left[Z_B - (Z_Z - X_B\theta_Y + Y_B\theta_X)\right](\theta_B - \theta_Z), \\
R &= \frac{1}{2}C\left(\dot{Z}_Z - X_1\dot{\theta}_Y + Y_1\dot{\theta}_X\right)^2 + \frac{1}{2}C\left(\dot{Z}_Z - X_2\dot{\theta}_Y + Y_2\dot{\theta}_X\right)^2 \\
&\quad + \frac{1}{2}C\left(\dot{Z}_Z - X_3\dot{\theta}_Y + Y_3\dot{\theta}_X\right)^2 \\
&\quad + \frac{1}{2}C\left(\dot{Z}_Z - X_4\dot{\theta}_Y + Y_4\dot{\theta}_X\right)^2 + \frac{1}{2}C_{\theta_Z}\dot{\theta}_Z^2.
\end{aligned} \tag{1}$$

Under the influence of multiple DOFs and damping, Lagrange's equation can be written as

$$\frac{d}{dt}\left(\frac{\partial T}{\partial \dot{q}_i}\right) - \frac{\partial T}{\partial q_i} + \frac{\partial R}{\partial \dot{q}_i} + \frac{\partial V}{\partial q_i} = F_i, \quad i = 1, 2, \ldots, n, \tag{2}$$

representing the $Z_Z, \theta_X, \theta_Y, \theta_Z, Z_B, \theta_B$ DOFs,

where F_i comprises the forces in all DOFs. Substituting (1) into (2), we can obtain the equation of motion for Z_Z, as follows:

$$\begin{aligned}
&M\ddot{Z}_Z + 4C\dot{Z}_Z + C\sum_{i=1}^{4}Y_i\dot{\theta}_X - C\sum_{i=1}^{4}X_i\dot{\theta}_Y \\
&\quad + 4KZ_Z + K_BZ_Z + K\sum_{i=1}^{4}Y_i\theta_X + K_BY_B\theta_X \\
&\quad - K\sum_{i=1}^{4}X_i\theta_Y - K_BX_B\theta_Y + \frac{1}{2}\delta\theta_Z - K_BZ_B - \frac{1}{2}\delta\theta_B \\
&= F_Z.
\end{aligned} \tag{3}$$

The equation of motion for θ_X is

$$\begin{aligned}
&I_X\ddot{\theta}_X + C\sum_{i=1}^{4}Y_i\dot{Z}_Z + C\sum_{i=1}^{4}Y_i^2\dot{\theta}_X - C\sum_{i=1}^{4}X_iY_i\dot{\theta}_Y \\
&\quad + K\sum_{i=1}^{4}Y_iZ_Z + K_BY_BZ_Z + K\sum_{i=1}^{4}Y_i^2\theta_X + K_BY_B^2\theta_X \\
&\quad - K\sum_{i=1}^{4}X_iY_i\theta_Y - K_BX_BY_B\theta_Y + \frac{1}{2}\delta Y_B\theta_Z \\
&\quad - K_BY_BZ_B - \frac{1}{2}\delta Y_B\theta_B = F_Z \cdot Y_T.
\end{aligned} \tag{4}$$

The equation of motion for θ_Y is

$$\begin{aligned}
&I_Y\ddot{\theta}_Y - C\sum_{i=1}^{4}X_i\dot{Z}_Z - C\sum_{i=1}^{4}X_iY_i\dot{\theta}_X + C\sum_{i=1}^{4}X_i^2\dot{\theta}_Y \\
&\quad - K\sum_{i=1}^{4}X_iZ_Z - K_BX_BZ_Z - K\sum_{i=1}^{4}X_iY_i\theta_X - K_BX_BY_B\theta_X \\
&\quad + K\sum_{i=1}^{4}X_i^2\theta_Y + K_BX_B^2\theta_Y - \frac{1}{2}\delta X_B\theta_Z + K_BX_BZ_B \\
&\quad + \frac{1}{2}\delta X_B\theta_B = -F_Z \cdot X_T.
\end{aligned} \tag{5}$$

The equation of motion for θ_Z is

$$I_Z \ddot{\theta}_Z + C_{\theta_Z} \dot{\theta}_Z + \frac{1}{2}\delta Z_Z + \frac{1}{2}Y_B\theta_X - \frac{1}{2}X_B\theta_Y + K_\theta\theta_Z + K_{\theta_Z}\theta_Z - \frac{1}{2}\delta Z_B - K_\theta\theta_B = F_{TY}\cdot X_T - F_{TX}\cdot Y_T. \quad (6)$$

The equation of motion for Z_B is

$$m\ddot{Z}_B - K_B Z_Z - K_B Y_B\theta_X + K_B X_B\theta_Y - \frac{1}{2}\delta\theta_Z + K_B Z_B + \frac{1}{2}\delta\theta_B = F_B. \quad (7)$$

The equation of motion for θ_B is

$$I_B\ddot{\theta}_B - \frac{1}{2}\delta Z_Z - \frac{1}{2}\delta Y_B\theta_X + \frac{1}{2}\delta X_B\theta_Y - K_\theta\theta_Z + \frac{1}{2}\delta Z_B + K_\theta\theta_B = M_B. \quad (8)$$

Using the above derivation process, we can obtain a 3D equation of motion for the rigid plate and vibration absorber system. As for the frequency responses in the system, we assume that $\{Z_Z, \theta_X, \theta_Y, \theta_Z, Z_B, \theta_B\} = \{\overline{Z}_Z e^{i\omega t}, \overline{\theta}_X e^{i\omega t}, \overline{\theta}_Y e^{i\omega t}, \overline{\theta}_Z e^{i\omega t}, \overline{Z}_B e^{i\omega t}, \overline{\theta}_B e^{i\omega t}\}$ and that the external force and moment are $\{F_Z(t), M_B(t)\} = \{\overline{F}_Z e^{i\omega t}, \overline{M}_B e^{i\omega t}\}$. As a result, the equations of motion of the 6 DOFs in the frequency domain can be written as the matrix below:

$$[A]\begin{Bmatrix}\overline{Z}_Z\\ \overline{\theta}_X\\ \overline{\theta}_Y\\ \overline{\theta}_Z\\ \overline{Z}_B\\ \overline{\theta}_B\end{Bmatrix} = \begin{Bmatrix}\overline{F}_Z\\ \overline{F}_Z Y_T\\ -\overline{F}_Z X_T\\ \overline{F}_{TY}X_T - \overline{F}_{TX}Y_T\\ \overline{F}_B\\ \overline{M}_B\end{Bmatrix} m, \quad (9)$$

where

$$[A] = \begin{bmatrix} -\omega^2 M + i\omega 4C + 4K + K_B & K_B Y_B & -K_B X_B & \frac{1}{2}\delta & -K_B & -\frac{1}{2}\delta \\ K_B Y_B & -\omega^2 I_X + i\omega 4CY_1^2 + 4KY_1^2 + K_B Y_B^2 & -K_B X_B Y_B & \frac{1}{2}\delta Y_B & -K_B Y_B & -\frac{1}{2}\delta Y_B \\ -K_B X_B & -K_B X_B Y_B & -\omega^2 I_Y + i\omega 4CX_1^2 + 4KX_1^2 + K_B X_B^2 & -\frac{1}{2}\delta X_B & K_B X_B & \frac{1}{2}\delta X_B \\ \frac{1}{2}\delta & \frac{1}{2}\delta Y_B & -\frac{1}{2}\delta X_B & -\omega^2 I_Z + i\omega C_{\theta_Z} + \left(K_\theta + K_{\theta_Z}\right) & -\frac{1}{2}\delta & -K_\theta \\ -K_B & -K_B Y_B & K_B X_B & -\frac{1}{2}\delta & K_B - \omega^2 m & \frac{1}{2}\delta \\ -\frac{1}{2}\delta & -\frac{1}{2}\delta Y_B & \frac{1}{2}\delta X_B & -K_\theta & \frac{1}{2}\delta & K_\theta - \omega^2 I_B \end{bmatrix}. \quad (10)$$

This enables us to obtain the frequency responses of the system using numerical methods and compare them with experiment results for verification.

3. Analysis of System Natural Frequencies

The above derivation process produced the equation of motion for the rigid plate and vibration absorber system. The equation of motion for the rigid plate without the HDBVA can be obtained by eliminating the terms of the HDBVA in the theoretical model. It should be noted that, for a rectangular plate, X_i and Y_i are symmetric, and, therefore, $\sum_{i=1}^{4} X_i = 0$ and $\sum_{i=1}^{4} Y_i = 0$. Furthermore, the frequency responses of the four DOFs Z_Z, θ_X, θ_Y, and θ_Z can be assumed to be $\{Z_Z, \theta_X, \theta_Y, \theta_Z\} = \{\overline{Z}_Z e^{i\omega t}, \overline{\theta}_X e^{i\omega t}, \overline{\theta}_Y e^{i\omega t}, \overline{\theta}_Z e^{i\omega t}\}$, and $F_Z(t) = \overline{F}_Z e^{i\omega t}$. As a result, the equations of motion for the four DOFs can be expressed as follows:

$$[A]\begin{Bmatrix}\overline{Z}_Z\\ \overline{\theta}_X\\ \overline{\theta}_Y\\ \overline{\theta}_Z\end{Bmatrix} = \begin{Bmatrix}\overline{F}_Z\\ \overline{F}_Z Y_T\\ -\overline{F}_Z X_T\\ \overline{F}_{TY}X_T - \overline{F}_{TX}Y_T\end{Bmatrix}, \quad (11)$$

where Matrix A can be written as

$$\begin{bmatrix} -\omega^2 M + i\omega 4C + 4K & 0 & 0 & 0 \\ 0 & -\omega^2 I_X + i\omega 4CY_1^2 + 4KY_1^2 & 0 & 0 \\ 0 & 0 & -\omega^2 I_Y + i\omega 4CX_1^2 + 4KX_1^2 & 0 \\ 0 & 0 & 0 & -\omega^2 I_Z + i\omega C_{\theta_Z} + K_{\theta_Z} \end{bmatrix}. \tag{12}$$

Thus, the numerical solutions of the frequency responses can be derived using the formula above. The analytical solution for the natural frequency of the system can also be obtained using a basic eigenmatrix. Suppose that $\{Z_Z, \theta_X, \theta_Y, \theta_Z\} = \{\overline{Z}_Z e^{\lambda t}, \overline{\theta}_X e^{\lambda t}, \overline{\theta}_Y e^{\lambda t}, \overline{\theta}_Z e^{\lambda t}\}$, which when substituted into the equation of motion for the rigid plate without a vibration absorber results in the following eigenmatrix:

$$\begin{bmatrix} \lambda^2 + \frac{4C}{M}\lambda + \frac{4K}{M} & 0 & 0 & 0 \\ 0 & \lambda^2 + \frac{12C}{M}\lambda + \frac{12K}{M} & 0 & 0 \\ 0 & 0 & \lambda^2 + \frac{12C}{M}\lambda + \frac{12K}{M} & 0 \\ 0 & 0 & 0 & \lambda^2 + \frac{3C_{\theta_Z}}{Ml^2}\lambda + \frac{4K_{\theta_Z}}{Ml^2} \end{bmatrix}, \tag{13}$$

where $4KY_1^2/I_X = ((12 \times 4KY_1^2)/M(2Y_1)^2) = 12K/M$, $4KX_1^2/I_Y = (12 \times 4KX_1^2)/M(2X_1)^2 = 12K/M$, $K_{\theta_Z}/I_Z = K_{\theta_Z}/(Ml^2/3) = 3K_{\theta_Z}/Ml^2$, and $I_Z = Ml^2/3$. Thus, the damped natural frequencies of the system are $\sqrt{(4K/M) - (2C/M)^2}$, $\sqrt{(12K/M) - (6C/M)^2}$, $\sqrt{(12K/M) - (6C/M)^2}$, and $\sqrt{(3K_{\theta_Z}/Ml^2) - (1.5C_{\theta_Z}/Ml^2)^2}$.

The analytical solutions for the undamped natural frequencies in each DOF are $\sqrt{4K/M}$, $\sqrt{12K/M}$, $\sqrt{12K/M}$, and $\sqrt{3K_{\theta_Z}/Ml^2}$. Substituting these results into the mass and spring coefficients of the vibrating main body enables us to derive the analytical solutions for the natural frequencies in each DOF. Take, for example, the rigid plate with a lateral groove (detailed in Table 1). The analytical solutions for the natural frequencies of DOFs Z_Z, θ_X, θ_Y, and θ_Z are 23.3909, 40.5142, 40.5142, and 5.9720 Hz, respectively. These results provide a valuable reference for further research.

4. Experimental Design of Vibrating System

The purpose of the following experiment was to verify the accuracy and feasibility of the HDBVA. Our primary focus involved measuring the amount of vertical vibration as well as the amount of rotation around the respective axes in the rigid plate vibration model. In these experiments, we considered three metal plates with a length of 300 mm, a width of 150 mm, and a height of 20 mm. Grooves were etched in three directions for the simulations; the model with a diagonal groove is presented in Figure 2. Our intention was to simulate and measure the damping effects of the vibration absorber sliding along grooves in various directions. The directions selected for the grooves were based on the results from previous studies [13–16]. Figure 3 illustrates the three types of slider that were fit into the grooves, enabling the vibration absorber (HDBVA) to slide freely. We applied a suitable amount of lubricant in the grooves to ensure that friction between the grooves and sliders did not affect the experiment results. Finally, we covered the grooves with a metal sheet (5 mm thick) with the same area dimensions as the rigid plate to prevent the sliders from leaving the grooves during violent vibrations. Figure 4 illustrates the proposed rigid plate HDBVA system. Two AR700-24 laser displacement gauges (Acuity) were placed at various positions to measure the amount of vertical vibration and rotation around the X-, Y-, and Z-axes to a precision of m^{-6}. The experimental procedure outlined in Figure 5 was repeated for various frequencies.

5. Results and Discussion

This study measured the amplitudes and amount of rotation in each DOF corresponding to different frequencies.

Table 1: Parameters in numerical simulations of rigid plate with vibration absorber.

Parameter	Symbol	Value
Mass of lateral groove plate (kg)	M	2.5
Mass of diagonal groove plate (kg)	M	2.0
Mass of longitudinal groove plate (kg)	M	1.8
Mass of D-HDBVA (kg)	m	0.05
Spring constant of the plate (kg/sec^2)	K	13500
Damping coefficient of plate (kg/sec)	C	11.8
Torsional spring constant of plate (kg·mm^2/sec^2)	K_{θ_Z}	33000000
Torsional damping coefficient of plate (kg·mm^2/sec)	C_{θ_Z}	11.8
Plate mass-moment-of-inertia in X-dir. (kg·mm^2)	I_X	4687.5
Plate mass-moment-of-inertia in Y-dir. (kg·mm^2)	I_Y	1171.875
Plate mass-moment-of-inertia in Z-dir. (kg·mm^2)	I_Z	5859.375
Coil spring constant of HDBVA (kg/sec^2)	K_B	2400
Coil spring torsional constant of HDBVA (kg/sec^2)	K_θ	2400

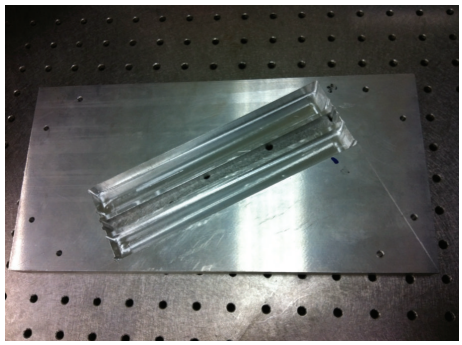

Figure 2: Picture of the diagonal groove rigid plate model.

We then plotted frequency response graphs for each DOF and compared the simulation results with and without the vibration absorber. In the experiments, the initial locations of the sliders included the near-force point (beneath the point at which the force was applied) and the far-from-force point (at the corner of the symmetrical quadrant) to confirm whether the vibration absorber provided optimal damping effects regardless of its initial position.

5.1. Results of Numerical Simulation. Figures 6 through 9 compare the results of numerical simulations involving the application of force to the corner of a rigid plate with lateral groove with the vibration absorber starting out at the near-force point and the far-from-force point as well as with no vibration absorber. Figure 6 compares the vertical amplitudes (mm); the bold line shows the simulation results with no vibration absorber, and "With HDBVA Far" and "With HDBVA Near" indicate the results when the vibration absorber is fixed at the far-from-force point and at the near-force point, respectively. Figures 7 through 9 compare the degree of rotation (rad) around the X-, Y-, and Z-axes. The vibration absorber is situated on the X-axis of the main body (the node line for θ_X DOF); therefore, it is clear that vibration absorber produces better damping effects at the far-from-force point in all the DOFs except θ_X. Furthermore, Figures 6 through 9 show that the resonance frequencies corresponding to the peaks derived from the numerical simulation are consistent with the analytical solutions of the natural frequencies of the rigid plate under conditions with no vibration absorber. These resonance frequencies were listed as 23.39 Hz, 40.51 Hz, 40.51 Hz, and 5.97 Hz in Section 3, thereby confirming that the numerical simulations are accurate. Comparisons also revealed that when the vibration absorber was located at the far-from-force point, it exerted superior vibration reduction. Due to the large number of parameter combinations in our experiments, we will not go into the details regarding the numerical simulations of the rigid plates with diagonal and longitudinal grooves. Nonetheless, the simulation results are presented with the experiment results in Section 5.2 (B).

Figures 6 and 8 also showed that the addition of the vibration absorber led to some fluctuation in a portion of the DOFs. Some unusual changes in amplitude occurred at various frequencies, such as between 30 Hz and 35 Hz, because these frequencies are the natural frequencies of the vibration absorber. As a result, when the natural frequency of the vibration absorber was reached, the rotation and vertical amplitudes of the vibration absorber significantly influenced the amplitudes of vibration in the main body. These results verify the feasibility of using the numerical simulation of rigid plates with vibration absorbers and provide a reference for subsequent experiments. The parameters of the rigid plates with different grooves are listed in Table 1. In Figure 8, the cases of "With HDBVAs." show higher amplitudes than the "No HDBVA" case in the frequency range of 30–35 Hz. It is because the natural frequencies of the HDBVAs are in that range. The higher amplitudes for HDBVAs are expected. However, in the frequencies near 40–50 Hz which is the θ_y-D.O.F. natural frequency, the case of "With HDBVA Far" demonstrates its better damping effect than the cases of "With HDBVA Near" and "No HDBVA". This also shows the superior vibration reduction of the "With HDBVA Far" cases.

Figure 6 was the comparison of vibration amplitudes of numerical simulation of Z_Z-D.O.F. It is the case of Figure 10(a) and with force applied on the end point (⊕) of the plate. Figure 10 shows 4 typical cases of groove in the main plate. The groove in Figures 10(a), 10(b), and 10(c) also denotes the node line for θ_x-D.O.F., end point force applied plate, and θ_y-D.O.F., respectively. The numerical simulations predict that the locations of the HDBVAs on the node lines (cases of Figures 10(a), 10(b), and 10(c)) showing worse damping effect than the case of Figure 10(d). This is probably due to the fact that the force (or absorber) applied on the node line cannot provide an effective antimoment to balance the vibration system. The HDBVA in the case of Figure 6 and "With HDBVA Near" is located on the θ_x-D.O.F. node line. It is even worse when the location of the HDBVA is on

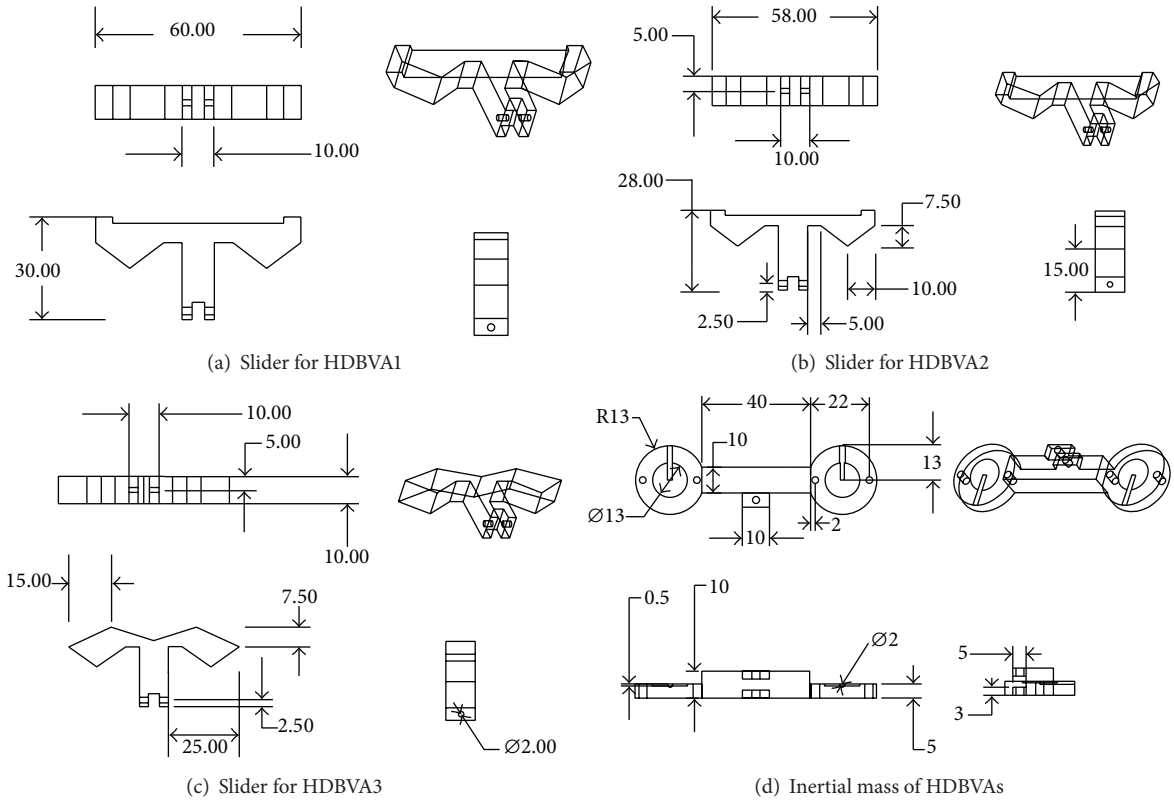

(a) Slider for HDBVA1 (b) Slider for HDBVA2

(c) Slider for HDBVA3 (d) Inertial mass of HDBVAs

Figure 3: Sliders and inertial mass for HDBVAs.

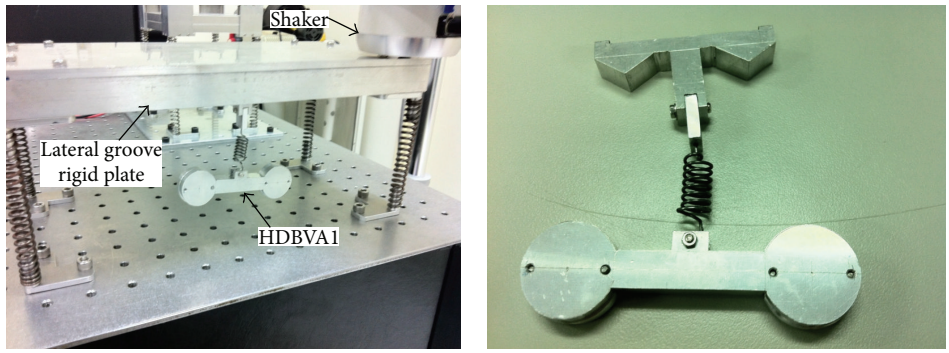

(a) Lateral groove rigid plate (b) HDBVA1

Figure 4: Experimental set up of HDBVA1 on lateral groove rigid plate.

the "same side" with the point of force application. Theoretically, this will increase the plate vibrating amplitudes for any D.O.F. It is also noted that the vibration absorber location was fixed in the theoretical cases. However, the experimental model allows the HDBVA to slide in the groove. Detailed discussion will be studied in Section 5.2 (B).

5.2. Experiment Results. The previous section only presents the numerical simulation results when the HDBVA is fixed at the ends of the grooves. To achieve self-adjusting balance and vibration reduction, we measured the effectiveness of various combinations of sliders and grooves. During the experiments, we located the point of force at a corner of the plate to simulate damping effects under extreme conditions. To identify the locations in which the vibration absorber provides the best damping effects, we recorded the slid displacement of the sliders and measured the amplitudes in the various DOFs after the sliders stopped moving. We then compared the results with those of numerical simulations.

(A) Observations of Sliding Balance in Experiments. This study investigated the damping effects of vibration absorbers equipped with three different sliders on grooves in three different directions, using two force application points. The combinations of groove direction and force application point are presented in Figure 10, where ⊕ marks the point of force,

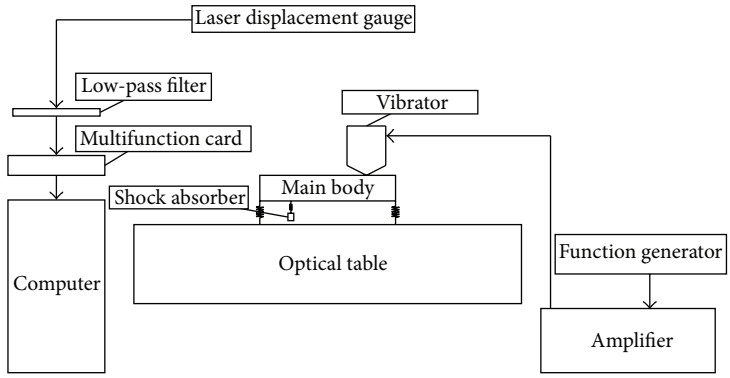

Figure 5: Schematic diagram of experimental setup.

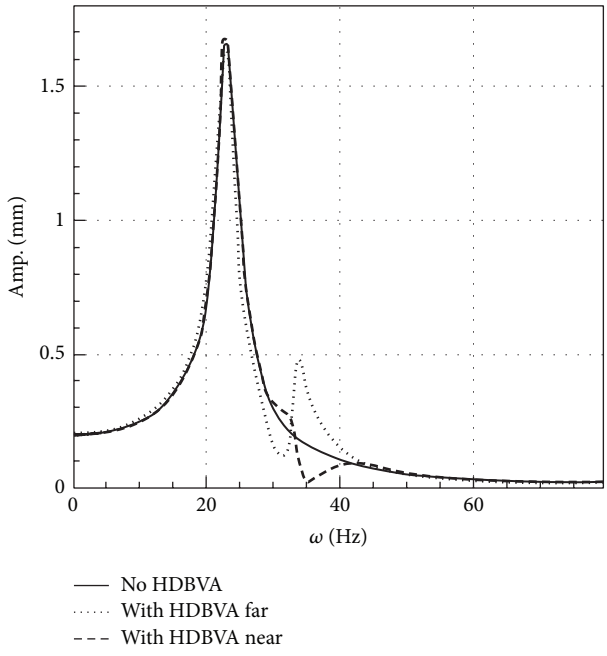

Figure 6: Numerical results of frequency response in Z_Z DOF with lateral groove.

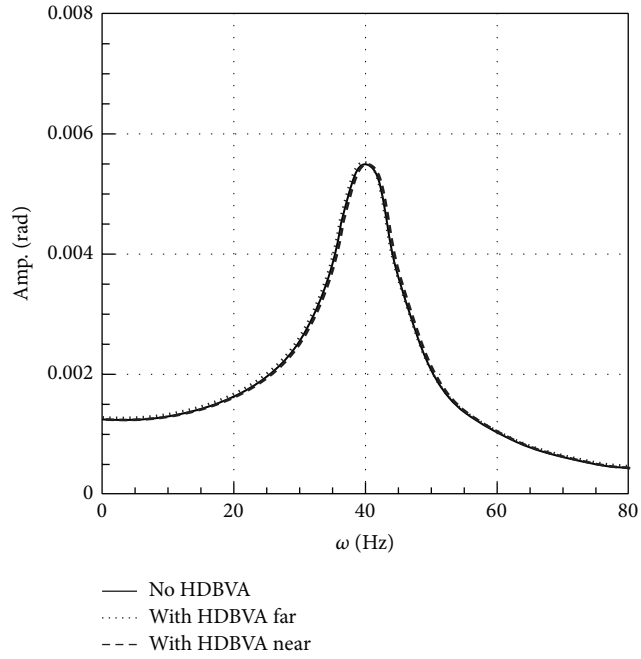

Figure 7: Numerical results of frequency response in θ_X DOF with lateral groove.

and F and N denote the far-from-force points and near-force points in the grooves. We first considered circumstances (a) through (c) in Figure 10, in which force was applied at the corner of the rigid plate. Once the slider stopped moving, we recorded its displacement. Due to the considerable amount of raw data we obtained, we present here only the results obtained using the lateral groove with three types of slider. The remainder of the data is graphically presented in the following figures. Table 2 contains the displacement records of the slider of HDBVA1 in lateral groove as in Figure 10(a). The F means that the slider ends up at the far-from-force point, N means that the slider ends up at the near-force point, and m means that the slider ends up in the middle of the groove. Displacement (cm) refers to the sliding distance of the slider, which, when divided by the length of the groove, yields the displacement percentage (%). The columns on the left present the results for the situation in which the slider started at the groove end near the force application point, whereas the columns on the right give the results for when the slider started at the groove end away from the force application point. It should be noted that between 30 Hz and 40 Hz, obvious sliding was observed, regardless of the initial location of the vibration absorber. This is because the natural frequency of the vibration absorber is within this range, such that the vibration absorber is forced to adjust its location to concentrate the vibrations on itself, thereby reducing the amplitude of vibration in the main body.

To further elucidate the sliding conditions of the three types of slider in the various types of groove, we divided the displacement records into two parts including in-range frequency (30–40 Hz) and out-range frequency (5–29 Hz and

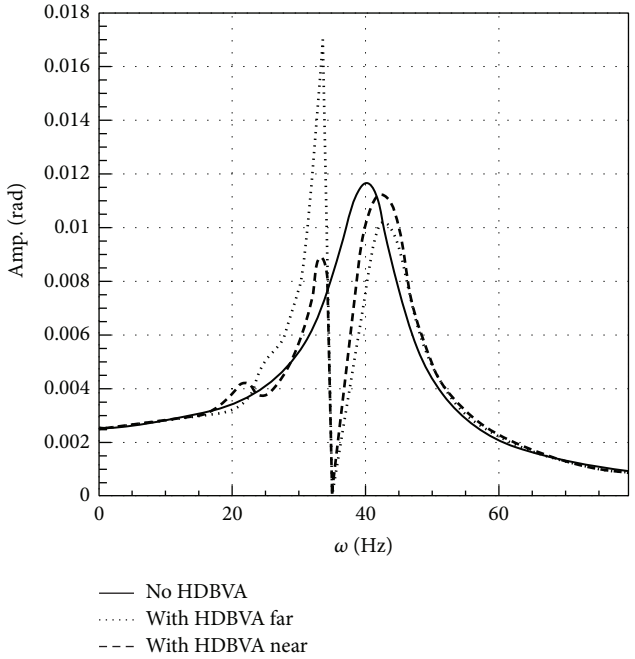

Figure 8: Numerical results of frequency response in θ_Y DOF with lateral groove.

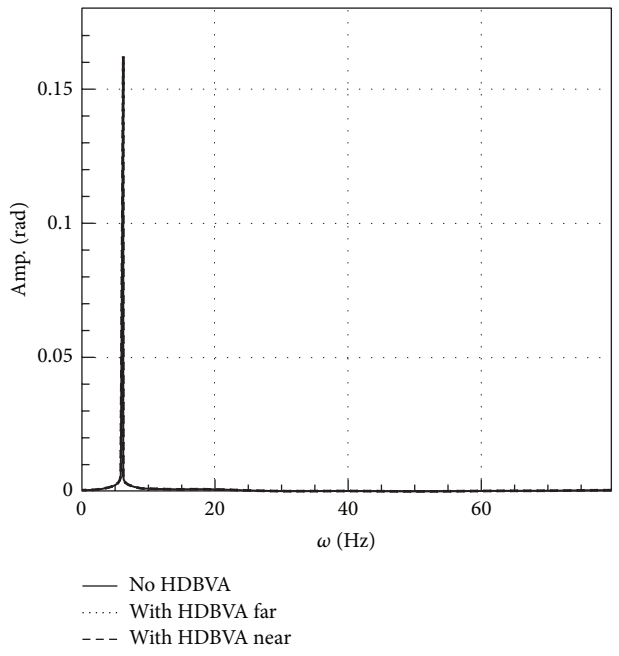

Figure 9: Numerical results of frequency response in θ_Z DOF with lateral groove.

41–50 Hz). The relationships between displacement percentage and the location of the slider after self-adjustment are presented in Figures 11 through 16. We further divided the sliding percentages into three groups: the near-force (N) group (less than 33%), the middle (m) group (33%–66%), and the far-from-force (F) group (over 66%). This allowed us to immediately see the distributions of the vibration absorber locations after sliding. In these graphs, the vertical axis measures the distance percentage between the initial and final locations of the vibration absorber. HDBVA1 denotes

Table 2: Slider displacement of HDBVA1 in lateral groove.

Hz	Starting at near-force pt.			Starting at far-from-force pt.		
	Stop Pos.	Disp./cm	Disp./%	Stop Pos.	Disp./cm	Disp./%
5	N	0	0	F	0	0
6	N	0	0	F	0	0
7	N	0	0	F	0	0
8	N	0	0	F	0	0
9	N	0	0	F	0	0
10	N	0	0	F	0	0
11	N	0	0	F	0	0
12	N	0	0	F	0	0
13	N	0	0	F	0	0
14	N	0	0	F	0	0
15	N	0	0	F	0	0
16	N	0	0	F	0	0
17	N	0	0	F	0	0
18	N	0	0	F	0	0
19	N	0	0	F	0	0
20	N	0	0	F	0	0
21	N	0	0	F	0	0
22	N	0	0	F	0	0
23	N	0	0	F	0	0
24	N	0	0	F	0	0
25	N	0	0	F	0	0
26	N	0	0	F	0	0
27	N	0	0	F	0	0
28	N	0	0	F	0	0
29	N	0	0	F	0	0
30	m	6.5	50.0	F	0	0
31	N	0	0	F	0	0
32	m	6.0	46.154	F	0	0
33	m	5.5	42.308	F	1.0	7.692
34	m	7.0	53.846	F	0	0
35	m	5.5	42.308	F	2.0	15.385
36	m	5.0	38.462	F	3.0	23.077
37	N	0	0	F	0	0
38	N	0	0	F	1.5	11.538
39	N	0	0	F	1.0	7.692
40	N	0	0	F	0	0
41	N	0	0	F	0	0
42	N	0	0	F	0	0
43	N	0	0	F	0	0
44	N	0	0	F	0	0
45	N	0	0	F	0	0
46	N	0	0	F	0	0
47	N	0	0	F	0	0
48	N	0	0	F	0	0
49	N	0	0	F	0	0
50	N	0	0	F	0	0

N = near-force, F = far-from-force, m = middle-of-groove.

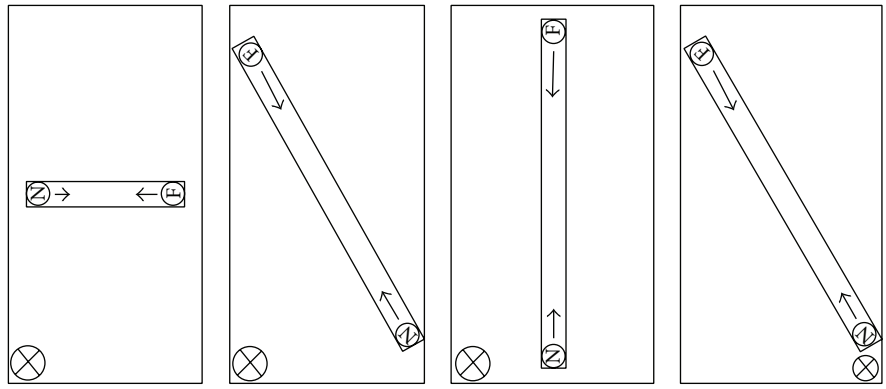

(a) Lateral groove (b) Diagonal (c) Longitudinal (d) Diagonal

Figure 10: Types of groove in the main body and location of force application in experiments.

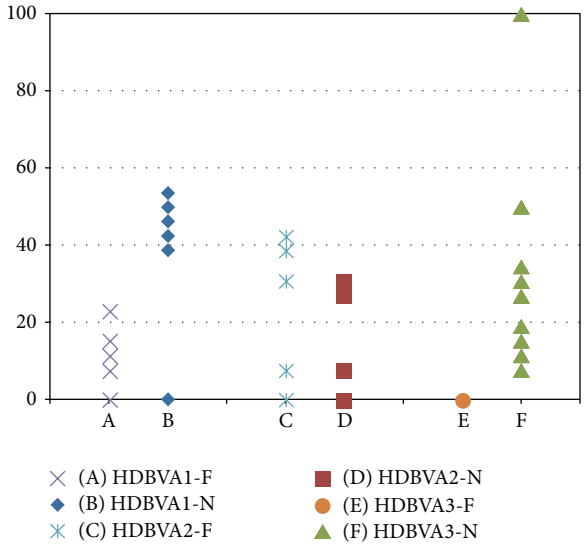

Figure 11: In-range slider displacement percentages of case Figure 10(a).

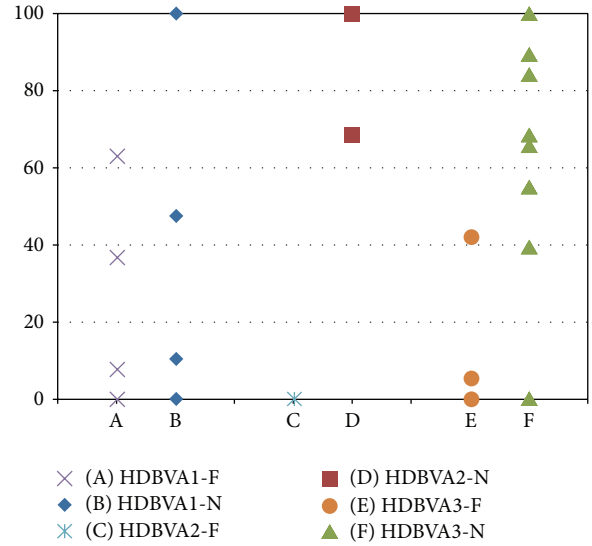

Figure 12: In-range slider displacement percentages of case Figure 10(b).

the slider of the HDBVA with the most friction, followed by HDBVA2 and HDBVA3. In the legend, *F* indicates that the initial location is at the far-from-force point, and *N* means that the initial location is at the near-force point. We labeled the various combinations using different letters (A~F on the horizontal axis) to differentiate them. Figures 11–13 display the in-range displacement percentages resulting from the different grooves, sliders, and initial locations of the vibration absorber, and Figures 14–16 exhibit the out-range results. The figures reveal that the movements of the vibration absorber are greater in in-range frequencies than in out-range frequencies. This is because the in-range frequencies are within the resonance frequency range of the main body, which leads to greater amplitudes and longer sliding distances. Obviously, the groove provided an extra DOF for the vibration absorber to slide in the in-range case.

In general, the vibration absorber slides a greater distance when it starts at the near-force point (*N*) than when it starts at the far-from-force point, as shown by B, D, and F in Figures 11–13. We speculate that this is due to the fact that the optimal damping position is generally near or at the far-from-force point. Thus, when the vibration absorber starts at the near-force point, it must move a greater distance to reach the optimal damping position and requires only a slight adjustment, if any, when it starts at the far-from-force point. The figures also show that the shape of the slider also influences its sliding capacity, due to the fact that the shape influences the amount of friction produced while sliding. In HDBVA3, the vibration absorber was initially situated at the optimal far-from-force point; however, it still moved slightly to seek the optimal damping position. In contrast, the vibration absorber in HDBVA1 did not slide as much as in HDBVA2 and HDBVA3. The slider in HDBVA1 generated the greatest friction; therefore, it barely moved in out-range frequency cases, as shown with A and B in Figures 14–16.

When force was applied at the corner of the plate, the diagonal groove was perfectly situated on the node line of the main body, which prevented the vibration absorber from

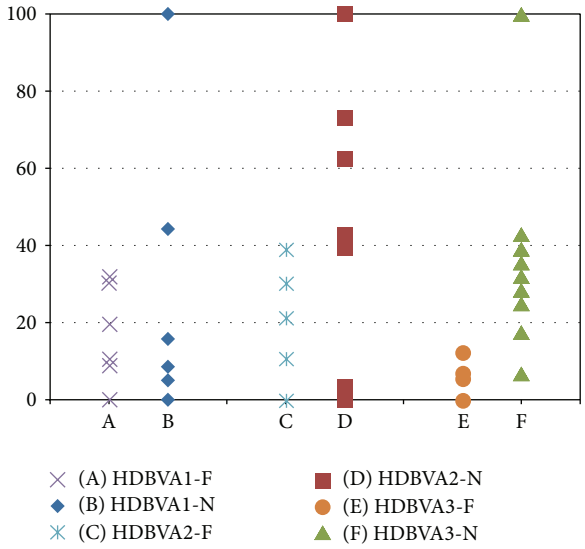

Figure 13: In-range slider displacement percentages of case Figure 10(c).

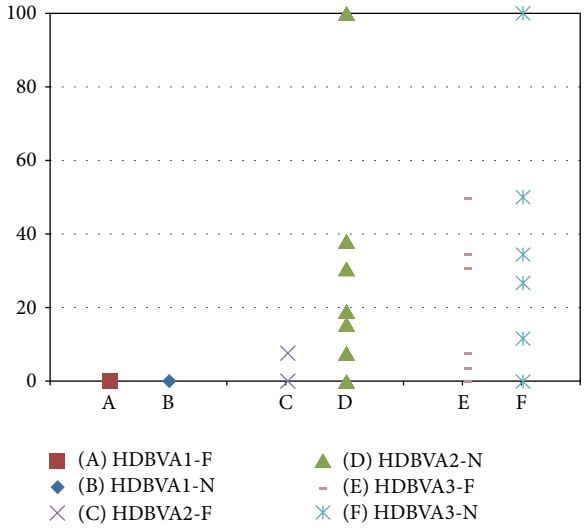

Figure 14: Out-Range slider displacement percentages of case Figure 10(a).

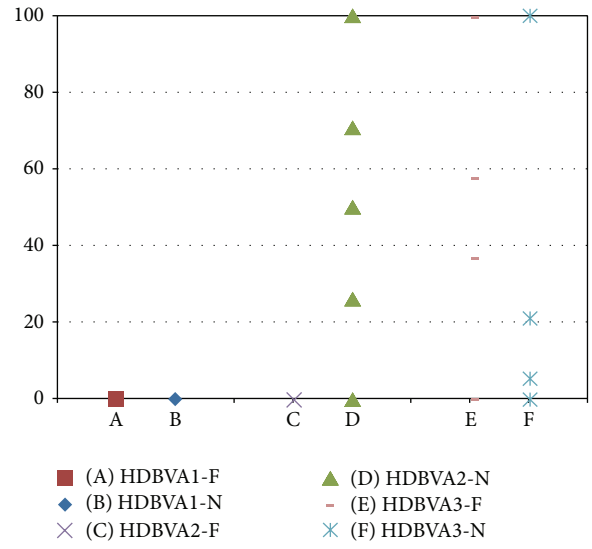

Figure 15: Out-Range slider displacement percentages of case Figure 10(b).

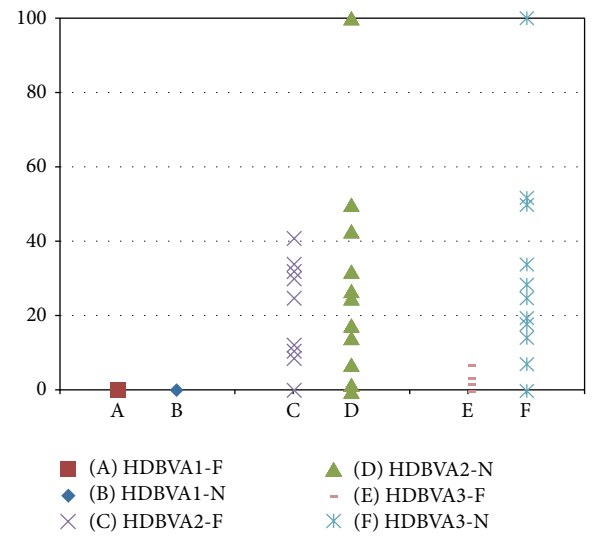

Figure 16: Out-Range slider displacement percentages of case Figure 10(c).

sliding in response to the external force. Thus, we performed an additional set of experiments with the diagonal groove, the various sliders, and the force application point situated at the end of the groove (Figure 10(d)). Similarly, we recorded the displacements of the vibration absorber in a table and plotted displacement percentage graphs. Figures 17 and 18 display the results of in-range and out-range frequencies, respectively. Comparisons of Figures 12 and 17 and Figures 15 and 18 presented the same conclusions as before, in which the vibration absorber slid for longer distances when it started at the near-force point (N) than when it started at the far-from-force point (F), as shown in Cases B, D, and F. Furthermore, the slider with less friction (HDBVA3) could move more easily than the slider with more friction (HDBVA1). These observations were made on the sliding circumstances of the vibration absorber. We discuss the damping effects of the vibration absorber in the following section.

Summarizing the experiment results leads to the following conclusions based on the apparent influence of slider friction on the damping effects of the vibration absorber. First, less friction enables the slider to find the optimal damping position and even enhances damping effects. When the vibration absorber starts at the near-force point, it frequently moves toward far-from-force point to seek a better damping position, regardless of slider type. Finally, the reduced sliding capability in cases with HDBVA1 prevents the vibration absorber from moving very much when it starts out at the far-from-force point. In contrast, the better balancing and optimal-position-seeking capabilities of HDBVA3 enable it

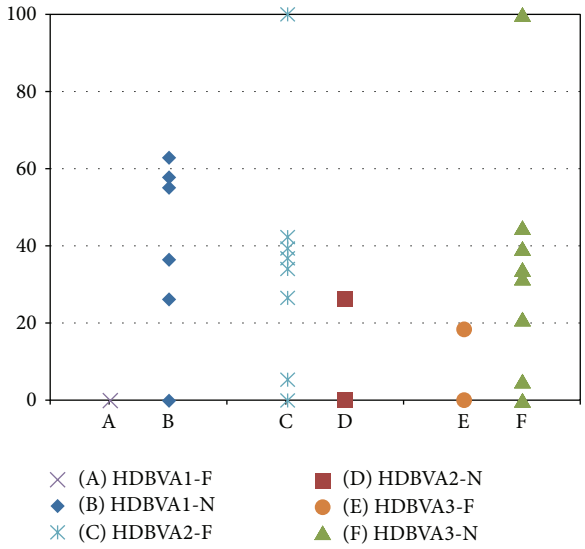

Figure 17: In-Range slider displacement percentages of case Figure 10(d).

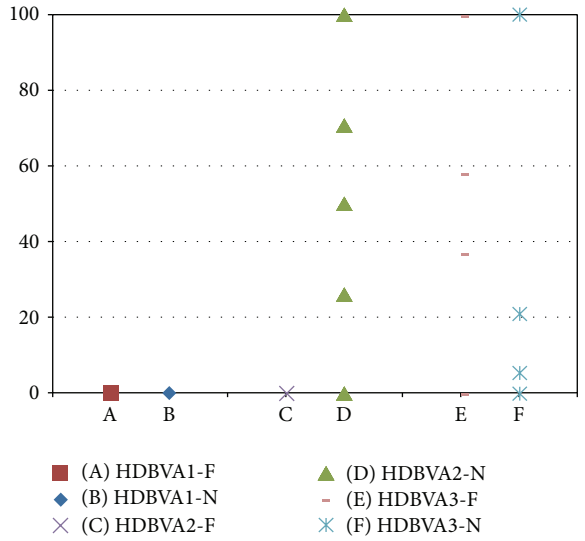

Figure 18: Out-Range slider displacement percentages of case Figure 10(d).

to slide and adjust its location more easily. The movement of HDBVA2 is not as smooth as that of HDBVA3; therefore, its sliding performance falls between that of the other two.

(B) Comparison of Experiment and Simulation Results. To verify the aforementioned theories and observation results, we compared the frequency response graphs created from the various combinations of grooves, sliders, and initial locations of the vibration absorber with those of the simulations. Figures 19, 20, 21, and 22 compare the frequency responses in the DOFs Z_Z, θ_X, θ_Y, and θ_Z when the vibration absorber starts at the near-force point in the lateral groove with the force application point in the corner of the rigid plate. Figure 19 is the comparison of Z_Z-D.O.F. vibration reduction effect of numerical simulation and experimental results. It

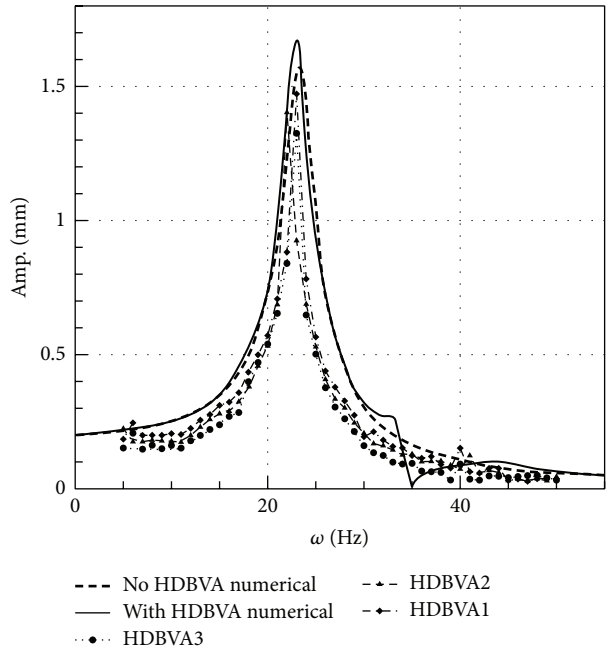

Figure 19: Frequency response of Z_Z DOF of case Figure 10(a), HDBVAs start at the near-force point.

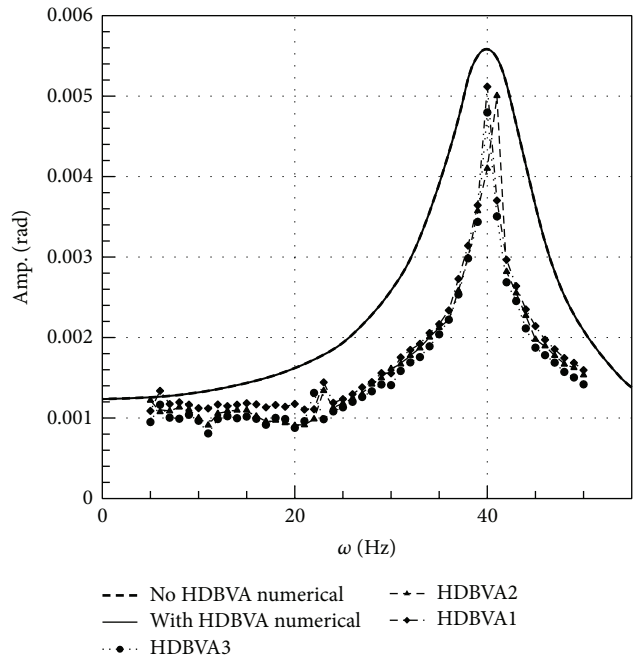

Figure 20: Frequency response of θ_X DOF of case Figure 10(a), HDBVAs start at the near-force point.

is the case of Figure 10(a) and near-force point. The curve denoted as "With HDBVA Num" is the same as the curve from Figure 6 "With HDBVA Near." It gives larger amplitude than "No HDBVA." It is due to the fact that the damper is located on the θ_x-D.O.F. node line and also on the "same side" with the force application point. Theoretically, this will increase

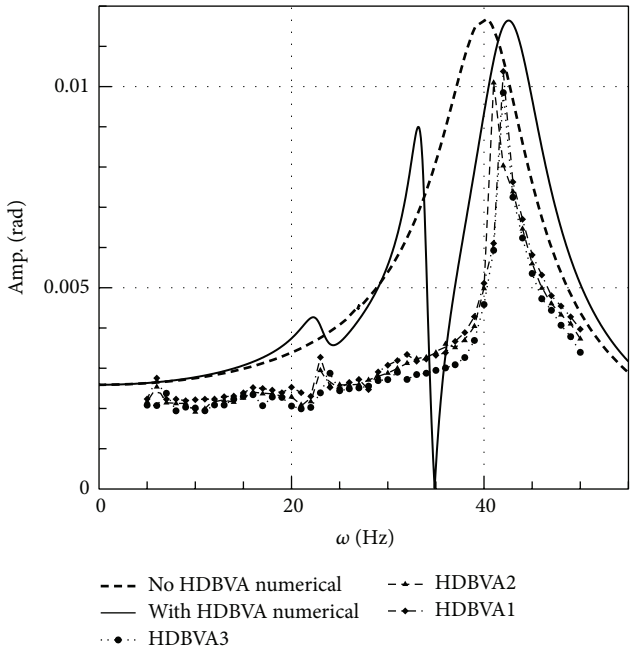

Figure 21: Frequency response of θ_Y DOF of case Figure 10(a), HDBVAs start at the near-force point.

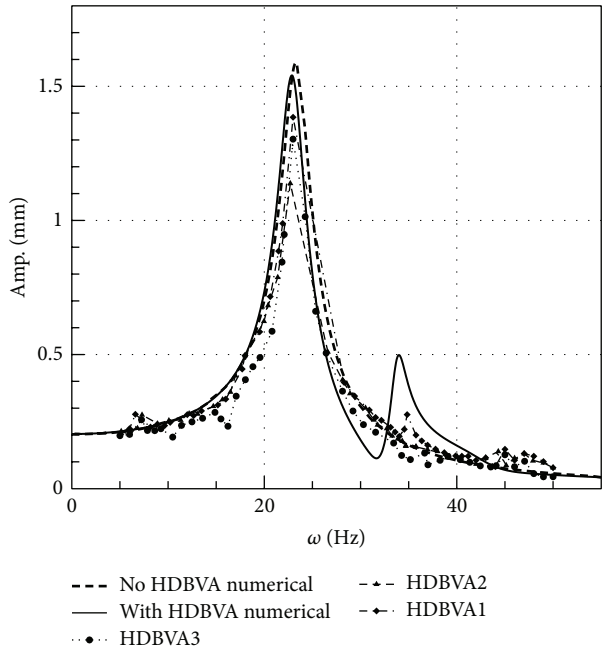

Figure 23: Frequency response of Z_Z DOF of case Figure 10(a), HDBVAs start at the far-from-force point.

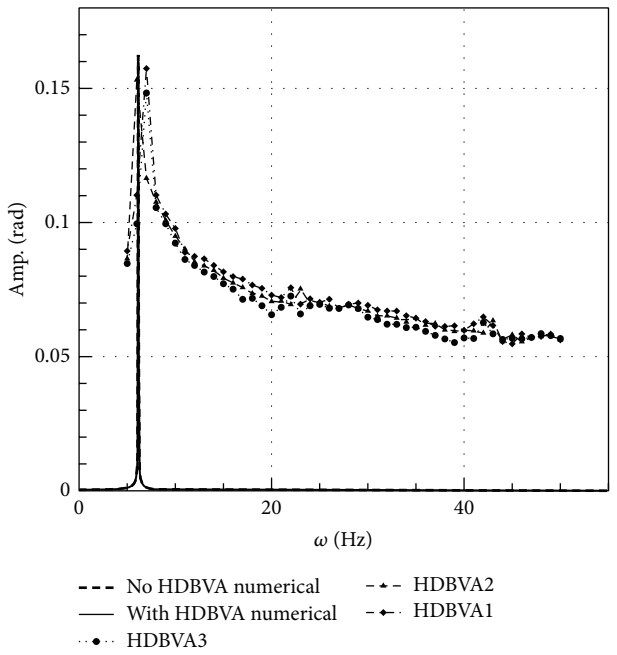

Figure 22: Frequency response of θ_Z DOF of case Figure 10(a), HDBVAs start at the near-force point.

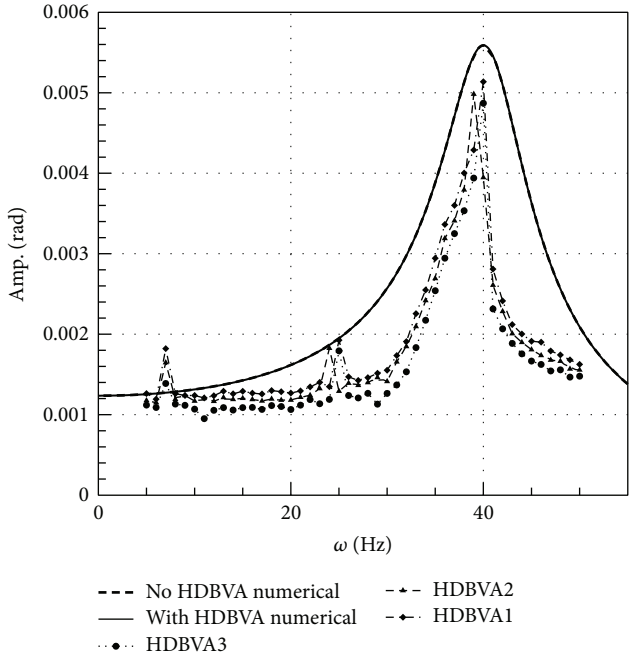

Figure 24: Frequency response of θ_X DOF of case Figure 10(a), HDBVAs start at the far-from-force point.

the plate vibrating amplitudes. Figure 20 is for the case of Figure 10(a) and in θ_x-D.O.F., which shows no significant damping effect, because the HDBVA is located on the x-axis (node line for θ_x-D.O.F.).

Figures 23, 24, 25, and 26 compare the frequency response results under the same conditions but with the vibration absorber starting from the far-from-force point. In terms of numerical simulations, the vibration absorber theoretically does not influence the frequency response of the θ_X DOF due to its relation with the node line. However, the experiments clearly demonstrate that various vibration absorber combinations still exhibit damping effects. Figure 25 is the comparison

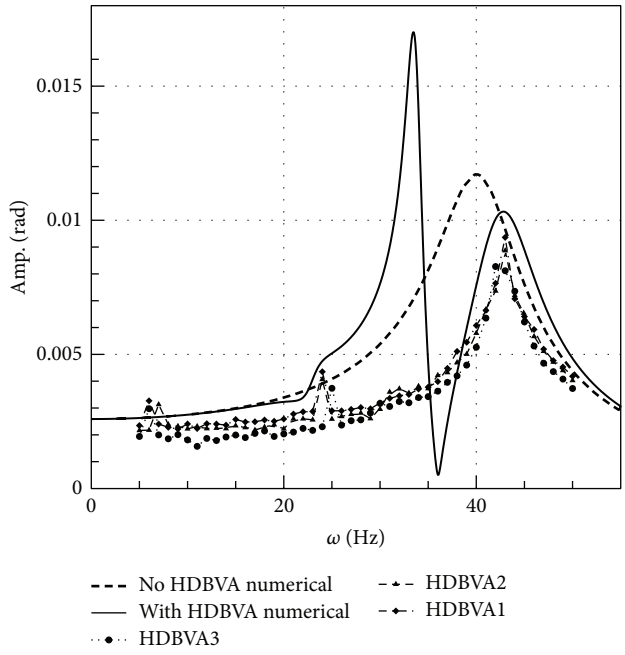

Figure 25: Frequency response of θ_Y DOF of case Figure 10(a), HDBVAs start at the far-from-force point.

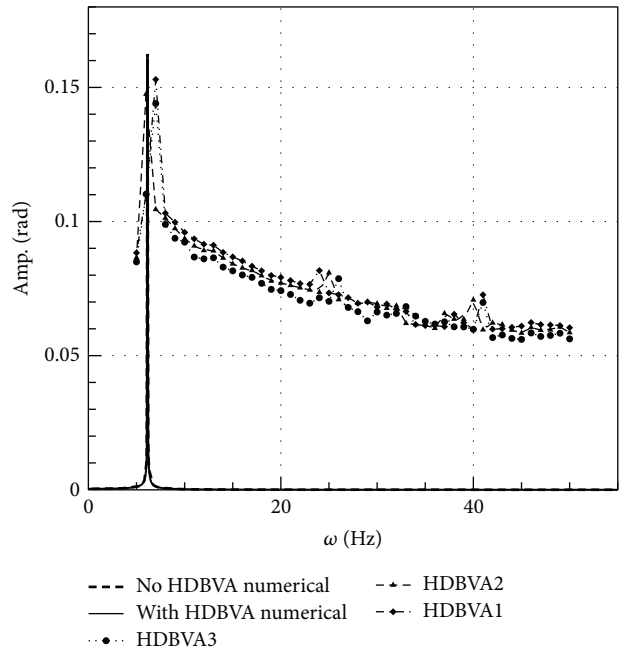

Figure 26: Frequency response of θ_Z DOF of case Figure 10(a), HDBVAs start at the far-from-force point.

of θ_y-D.O.F. vibration effect of numerical simulation and experimental results. It is for the case of Figure 10(a) and far-from-force point. The curve denoted as "With HDBVA Num" is the same as the curve from Figure 8 "With HDBVA Far." The case of "With HDBVA Num" shows higher amplitudes than the "No HDBVA" case in the frequency range of 30–35 Hz. This is because the natural frequencies of the HDBVAs

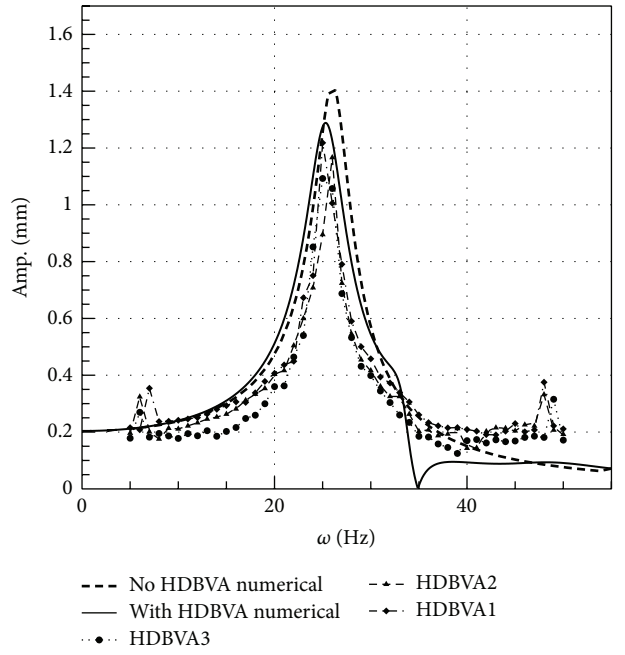

Figure 27: Frequency response of Z_Z DOF of case Figure 10(d), HDBVAs start at the near-force point.

are in that range. The higher amplitudes of HDBVAs are expected. However, in the range of the θ_y-D.O.F. natural frequency (about 40–50 Hz), the case of "With HDBVA Num Far" demonstrates its better damping effect than the case of "No HDBVA." Due to the word limit, we will not go into the cases with the diagonal and longitudinal grooves at length; however, the damping effects of these cases are compared and displayed in the tables. One observation worth mentioning concerns the setup with the force application point situated at the end of the diagonal groove (see Figure 10(d)).

Figures 27 through 30 and Figures 31 through 34 compare the frequency response results when the vibration absorber started at the near-force point and the far-from-force point, respectively. Figures 32 and 33 are for the case of Figure 10(d)—diagonal groove plate and far-from-force point. The HDBVA is not located on the node line in this case. Again, the natural frequencies for the HDBVAs are around 30–35 Hz and for the plate's θ_x- and θ_y-D.O.F. are around 40–50 Hz. The case of "With HDBVA Num" showed higher amplitudes than the "No HDBVA" case in the frequency range of 30–35 Hz. This is because the natural frequencies of the HDBVAs are in that range. The higher amplitudes of HDBVAs are expected. However, in the range of the θ_x- (Figure 32) and θ_y-D.O.F. (Figure 33) natural frequencies (about 40–50 Hz), the cases of "With HDBVA Num Far" demonstrate the better damping effect than the cases of "No HDBVA." We also noted that in the HDBVA's natural frequency (30–35 Hz), there are always amplitude peaks in the numerical results. The far-from-force point HDBVA case always shows higher amplitude than the near-force point case in that frequency range. On the other hand, in the cases of corresponding natural frequencies of θ_x- and θ_y-D.O.F. (around 40–50 Hz), the far-from-force point HDBVA performs better damping

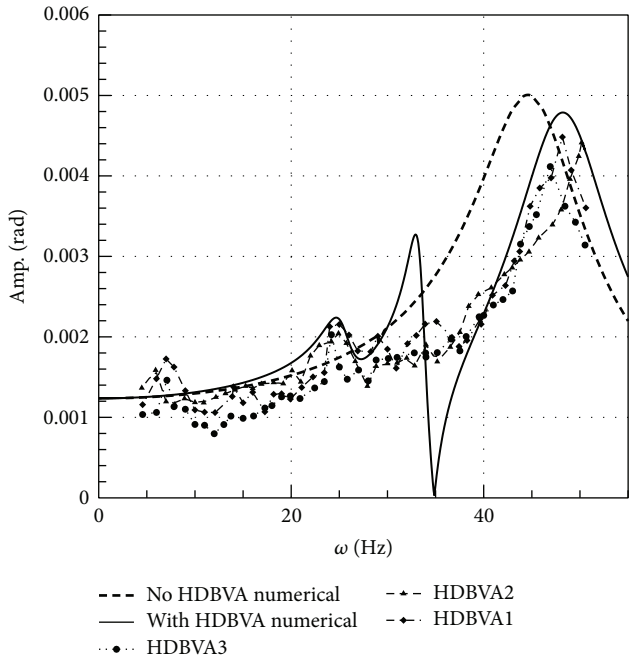

Figure 28: Frequency response of θ_X DOF of case Figure 10(d), HDBVAs start at the near-force point.

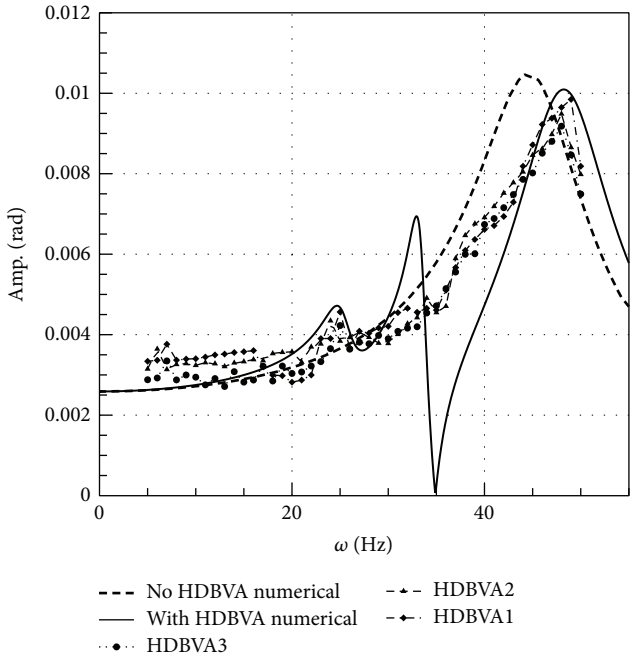

Figure 29: Frequency response of θ_Y DOF of case Figure 10(d), HDBVAs start at the near-force point.

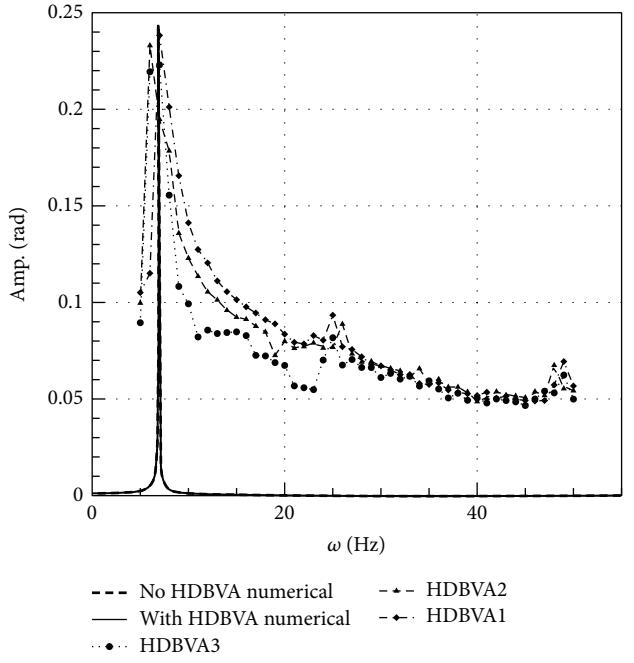

Figure 30: Frequency response of θ_Z DOF of case Figure 10(d), HDBVAs start at the near-force point.

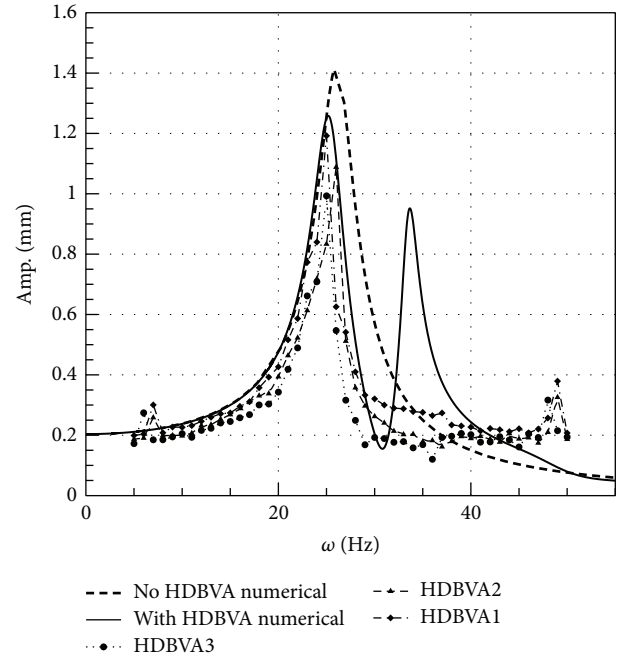

Figure 31: Frequency response of Z_Z DOF of case Figure 10(d), HDBVAs start at the far-from-force point.

effect than the near-force point HDBVA. Figures 28 and 32 and Figures 29 and 33 demonstrate this phenomenon. This may be due to the fact that the HDBVAs vibrate with larger amplitudes and absorb more energy to damp out the main plate vibration amplitudes in the cases of far-from-force point than the cases of near-force point. However, the true damping of the HDBVA spring may absorb some energy from the system in the frequencies between 30 and 35 Hz. Therefore, the experimental results show less vibration amplitudes than the numerical simulations that exclude HDBVAs damping. These graphs also show that the natural frequencies and analytical solutions derived from the experiments are more or

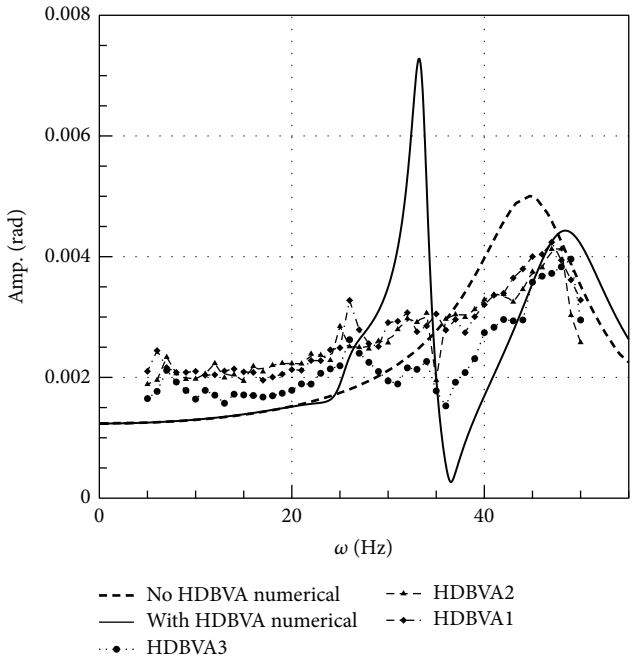

Figure 32: Frequency response of θ_X DOF of case Figure 10(d), HDBVAs start at the far-from-force point.

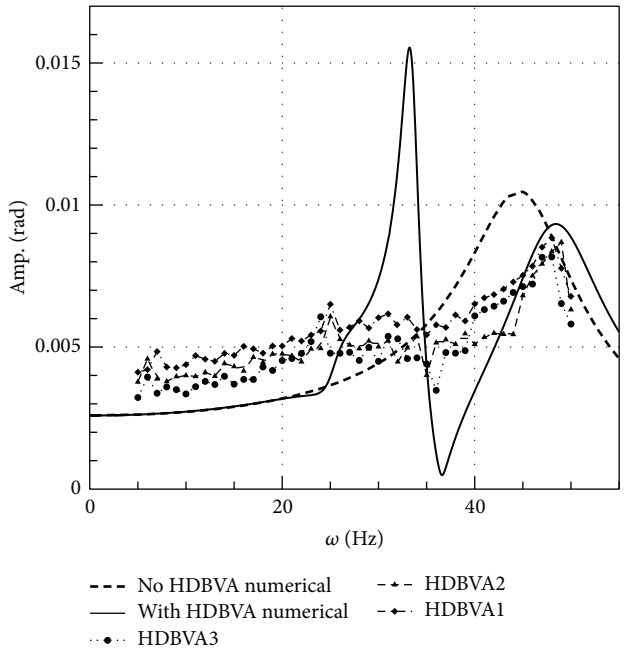

Figure 33: Frequency response of θ_Y DOF of case Figure 10(d), HDBVAs start at the far-from-force point.

less consistent with those in the simulation results. However, upon closer inspection, a number of slight peaks other than those near the theoretical natural frequencies appeared in the experiment results. We speculate that the decoupling of the DOFs during the theoretical derivation caused us to overlook the coupling factors between the vertical (Z-axis) vibrations and the rotation around the Z-axis (the θ_Z DOF). Consequently, the simulations excluded this coupling phenomenon, which appeared in the experiment results. It should also be noted that in the numerical simulations with a vibration absorber, the vibration absorber was fixed either at the far-from-force point or the near-force point, whereas the experiment results were obtained after the vibration absorber reached the optimal damping position and stopped sliding.

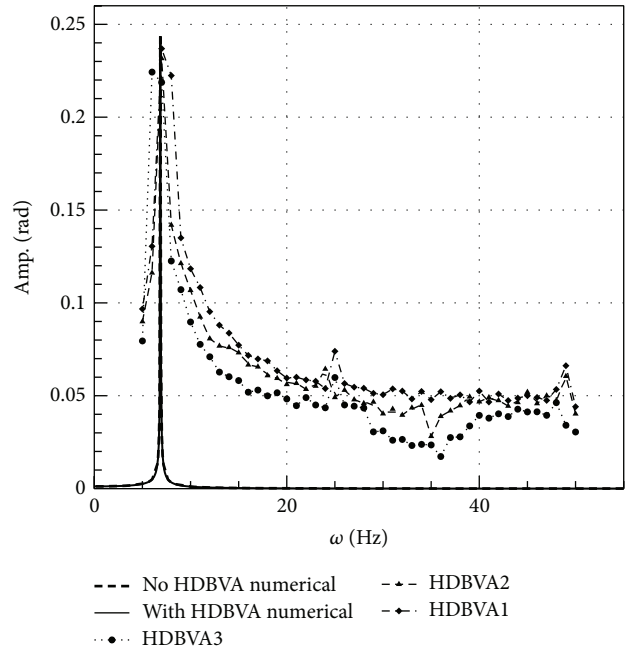

Figure 34: Frequency response of θ_Z DOF of case Figure 10(d), HDBVAs start at the far-from-force point.

Finally, to identify the groove and slider combination capable of providing the best damping effects, we normalized the results for comparison by dividing the natural frequency amplitudes in the experiment results by the amplitudes corresponding to the natural frequencies without the vibration absorber. The results displayed in Table 3 show that the best damping effects were obtained when force was applied at the end of the diagonal groove and the vibration absorber started at the far-from-force point with HDBVA3. We also normalized and compared the amplitudes resulting from the combinations at working frequencies (away from the natural frequency), the results of which are presented in Table 4. Observations and comparisons of the displacement records indicate that the amplitudes derived in the rigid plate experiments with a vibration absorber were smaller than the theoretical amplitudes in the numerical simulations in all DOFs, which demonstrates that the proposed designs in this study are capable of effectively dampening vibrations. Overall, using the same groove and external force, the vibration absorber mounted with HDBVA3 provided better damping effects than those with HDBVA1 and HDBVA2. In addition, when the vibration absorber slides to its optimal damping position, the measured amplitudes are significantly smaller.

In summary of the various graphs, the fact that the vibration absorber slides to different locations when subjected to

Table 3: Damping effects of groove and slider combinations (normalized).

	Case of Figure 10(a)	Case of Figure 10(b)	Case of Figure 10(c)	Case of Figure 10(d)
No HDBVA Num.	1	1	1	1
With HDBVA Num.	0.964269	1.003597	0.969740	0.908190
No HDBVA Expt.	0.940905	0.990377	0.951089	0.884846
HDBVA1-F	0.882411	0.954460	0.908507	0.875365
HDBVA1-N	0.923682	0.960480	0.951822	0.914288
HDBVA2-F	0.852047	0.936689	0.869267	0.840238
HDBVA2-N	0.896569	0.934389	0.921326	0.871497
HDBVA3-F	0.821092	0.889291	0.840896	0.795235
HDBVA3-N	0.860223	0.898586	0.889299	0.863010

Table 4: Damping effects of groove and slider combinations (away from natural frequency and normalized).

	Case of Figure 10(a)	Case of Figure 10(b)	Case of Figure 10(c)	Case of Figure 10(d)
No HDBVA Num.	1	1	1	1
With HDBVA Num.	0.891357	1.078969	0.953960	0.778815
No HDBVA Expt.	0.893914	0.964573	0.831144	0.756950
HDBVA1-F	0.686620	0.920159	0.834284	0.695305
HDBVA1-N	0.748457	1.048351	0.834214	0.736764
HDBVA2-F	0.759010	0.974331	0.736906	0.733996
HDBVA2-N	0.683924	0.709284	0.806611	0.682448
HDBVA3-F	0.681466	0.948458	0.812164	0.662156
HDBVA3-N	0.711264	0.862596	0.821613	0.708150

forces at different points proves that the proposed design is more flexible than a fixed vibration absorber by enabling self-adjustment to achieve optimal damping according to the working environment. Moreover, a diagonal design with the groove passing through the force application point was shown to be the best damping design. The friction produced by the sliding of the vibration absorber also has significant influence on the capacities of the vibration absorber with regard to damping and seeking the optimal damping position. Reducing the friction provides the slider with greater freedom to move within the groove, which enhances the sensitivity of the vibration absorber in locating the ideal damping location. Furthermore, it can prevent the occurrence of more severe vibrations when the vibration absorber reaches its natural frequency.

6. Conclusion

The objective of this study was to design a self-adjusting, structurally simple, and inexpensive passive damping system that does not need to be structurally altered to deal with changes in the working environment. The vibration absorber in the proposed system is able to adjust its location according to changes in the applied external force in order to achieve the best damping effects. We first used analytical solutions and numerical methods to obtain the natural frequencies, amplitudes, and torsion angles of the various vibration models in each DOF. After comparing the results, we physically constructed vibration models for experimentation and compared the experiment results with those derived in the numerical simulations.

Many DOFs were affected by vibrations within the main body, and the external force was not fixed. As a result, the placement of a single vibration absorber in one corner of the rigid plate would not be an optimal design as it would only be able to reduce the amplitudes in a single DOF. The hybrid vibration absorber proposed in this study is able to adjust its location in response to changes in the working environment, thereby achieving superior damping effects in all DOFs by combining the advantages of active and passive vibration absorber. We also discovered that sliders with smaller friction provide the best damping results by facilitating position-seeking capabilities. In conditions with only a single vibration absorber and changing external force, designs that enable the vibration absorber to move freely along a groove provide better damping effects than those in which the vibration absorber is fixed. A diagonal design with the groove passing through the force application point and the vibration absorber starting at the far-from-force point constitute the best damping design.

Conflict of Interests

The authors declare that there is no conflict of interests regarding the publication of this paper.

References

[1] V. I. Babitsky and A. M. Veprik, "Damping of beam forced vibration by a moving washer," *Journal of Sound and Vibration*, vol. 166, no. 1, pp.77–85, 1993.

[2] C. P. Chao, C.-K. Sung, and C.-C. Wang, "Dynamic analysis of the optical disk drives equipped with an automatic ball balancer with consideration of torsional motions," *Journal of Applied Mechanics*, vol. 72, no. 6, pp. 826–842, 2005.

[3] C.-P. Chao, C.-K. Sung, and H.-C. Leu, "Effects of rolling friction of the balancing balls on the automatic ball balancer for optical disk drives," *Journal of Tribology*, vol. 127, no. 4, pp. 845–856, 2005.

[4] C.-J. Lu and C.-H. Hung, "Stability analysis of a three-ball automatic balancer," *Journal of Vibration and Acoustics*, vol. 130, no. 5, Article ID 051008, 7 pages, 2008.

[5] J. P. Den Hartog, *Mechanical Vibration*, McGraw–Hill, 1947.

[6] A. F. Vakakis and S. A. Paipetis, "The effect of a viscously damped dynamic absorber on a linear multi-degree-of-freedom system," *Journal of Sound and Vibration*, vol. 105, no. 1, pp. 49–60, 1986.

[7] L. Zuo and S. A. Nayfeh, "Minimax optimization of multi-degree-of-freedom tuned-mass dampers," *Journal of Sound and Vibration*, vol. 272, no. 3–5, pp. 893–908, 2004.

[8] J. W. Heo, J. Chung, and J. M. Park, "Vibration and noise reduction of an optical disk drive by using a vibration absorber," *IEEE Transactions on Consumer Electronics*, vol. 48, no. 4, pp. 874–878, 2002.

[9] J. Chung, "Vibration absorber for reduction of the in-plane vibration in an optical disk drive," *IEEE Transactions on Consumer Electronics*, vol. 50, no. 2, pp. 552–557, 2004.

[10] S. T. Wu, Y. R. Chen, and S. S. Wang, "Two-degree-of-freedom rotational-pendulum vibration absorbers," *Journal of Sound and Vibration*, vol. 330, no. 6, pp. 1052–1064, 2011.

[11] S. Wu and P. Siao, "Auto-tuning of a two-degree-of-freedom rotational pendulum absorber," *Journal of Sound and Vibration*, vol. 331, no. 13, pp. 3020–3034, 2012.

[12] Y.-R. Wang and C.-M. Chang, "Elastic beam with nonlinear suspension and a dynamic vibration absorber at the free end," *Transactions of the Canadian Society for Mechanical Engineering*, vol. 38, no. 1, pp. 107–137, 2014.

[13] Y.-R. Wang and T.-H. Chen, "The vibration reduction analysis of a rotating mechanism deck system," *Journal of Mechanics*, vol. 24, no. 3, pp. 253–266, 2008.

[14] Y.-R. Wang and M.-S. Chang, "On the vibration reduction of a nonlinear support base with dual-shock-absorbers," *Journal of Aeronautics, Astronautics and Aviation A*, vol. 42, no. 3, pp. 179–190, 2010.

[15] Y.-R. Wang and H.-L. Chang, "The effect of a vibration absorber on a nonlinear two-dimensional system in vibration reduction," *Journal of Emerging Trends in Engineering and Applied Sciences*, vol. 1, no. 1, pp. 60–71, 2010.

[16] Y. R. Wang and S. W. Chen, "Study of the positions of multiple dampers in a dual-plate mechanism for vibration reduction," *Journal of Aeronautics, Astronautics and Aviation A*, vol. 45, no. 2, pp. 121–134, 2013.

[17] Y.-R. Wang and H.-S. Lin, "Stability analysis and vibration reduction for a two-dimensional nonlinear system," *International Journal of Structural Stability and Dynamics*, vol. 13, no. 5, Article ID 1350031, 2013.

[18] Y.-R. Wang and K.-E. Hung, "Damping effect of pendulum tuned mass damper on vibration of two-dimensional rigid body," *International Journal of Structural Stability and Dynamics*, vol. 15, no. 2, Article ID 1450041, 37 pages, 2015.

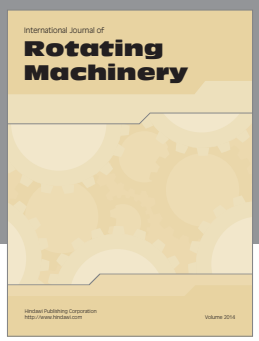

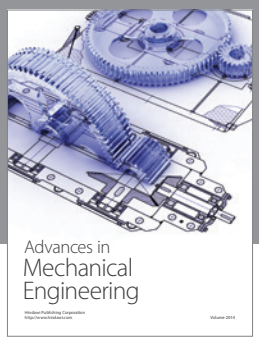

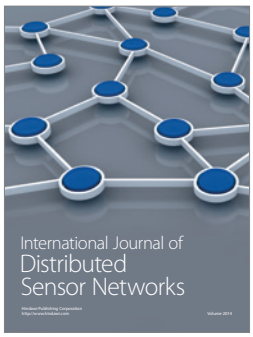

Hindawi
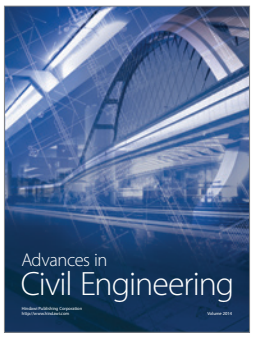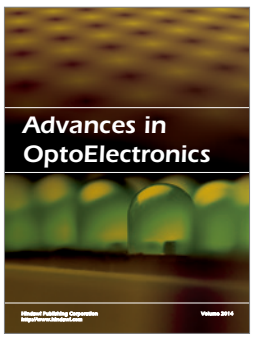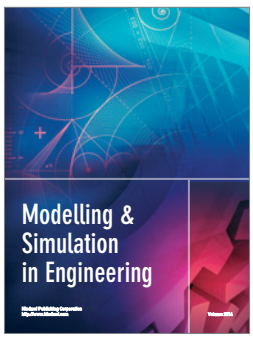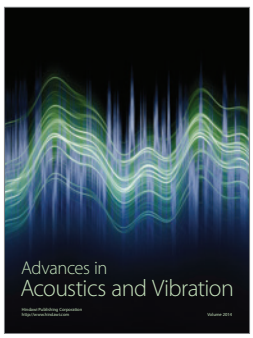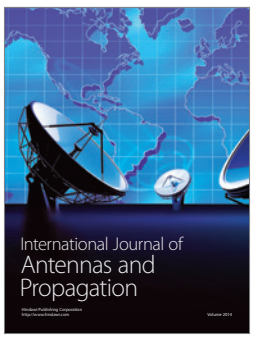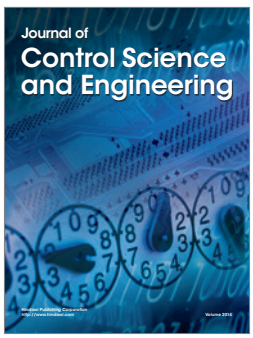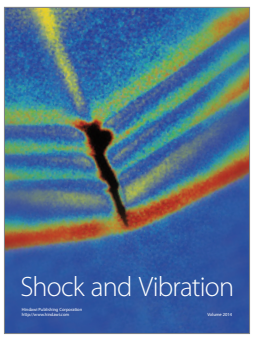
Submit your manuscripts at
http://www.hindawi.com